Defects in nematic membranes can buckle into pseudospheres

John R. Frank[*] and Mehran Kardar

Massachusetts Institute of Technology, Cambridge, Massachusetts 02139, USA
(Received 3 November 2007; published 15 April 2008)

Many factors influence the shapes of living and manufactured membranes. In addition to boundary conditions, surface tension, and curvature, the ordering of particles embedded in or attached to a membrane can strongly influence its equilibrium shape. As a simple model of such ordering, we consider rodlike particles that align to form a so-called nematic phase in the plane of the membrane. We call any sheet with such embedded orientational order a nematic membrane. Nematic membranes can occur in biological cells, liquid crystal films, manufactured materials, and other soft matter systems. By formulating the free energy of nematic films using tensor contractions from differential geometry, we elucidate the elastic terms allowed by symmetry, and indicate differences from hexatic membranes. We find that topological defects in the orientation field can cause the membrane to buckle over a size set by the competition between surface tension and in-plane elasticity. In the absence of bending rigidity the resulting shape is universal, known as a parabolic pseudosphere or a revolved tractrix. This buckling is the two-dimensional analog of the bent cores of line defects that are frequently observed in bulk nematic liquid crystals. Bending costs oppose such buckling and modify the shape in a predictable manner. In particular, the anisotropic rigidities of nematic membranes lead to different shapes for aster and vortex defects, in principle enabling measurement of couplings specific to nematic membranes.

PACS number(s): 61.30.Jf, 46.70.Hg, 87.16.D−, 68.47.Pe

I. INTRODUCTION

The fascinating shapes of membranes and thin films are often the result of geometry and topology rather than particular chemical reactions or a unique tuning of parameters. Energy dissipation under geometrical and topological constraints can guide a system into equilibrium forms and patterns that are common among many systems with a wide range of microscopic components. One category of such constraints results from the alignment of filaments or rodlike particles adhered to a membrane. Regardless of the detailed chemistry of the membrane and particles, such a system has global constraints that influence its shape. Topological (cowlicklike) defects arise naturally in the aligned filaments; the relaxation of these vortex- and star-shaped structures influences the overall shape of the membrane.

To better understand these patterns and their effect on the shapes of living cells and other condensed matter systems, we develop a simple model that idealizes many aspects of real membranes. We treat the membrane as an infinitely thin surface characterized only by its curved shape, and represent the filaments by a vector field in the tangent plane of the surface. This simplified model is known as a "nematic membrane."

Thus, a nematic membrane describes any flexible sheet incorporating ordered rodlike constituents. For example, thin films of smectic-*C* liquid crystals are nematic membranes [1–5]. Also, recently developed sheets of carbon nanotubes have nematic character [6,7]. Nematic order arises in lipid membranes with inclusions [8] and in the cell cytoskeleton, e.g. during mitosis [9]. Interestingly, *in vitro* experiments on mixtures of cytoskeletal filaments and protein motors observe topological defects (asters and vortices), which spontaneously self-organize into a variety of patterns [10–12]. These experiments, and related simulations, use *flat* geometries with various boundary conditions [13,14]. Similar topological defects influence the shapes of real cells. For example, cells of the alga *Bryopsis* sprout branches out of vortex-shaped defects that appear naturally in their cell wall of cellulose microfibrils [15]. To take a step toward understanding such living and *in vitro* systems, we consider equilibrium shapes around defects in deformable nematic membranes.

We show that topological defects can buckle the membrane. This has similarities to two other systems. One is bulk nematic liquid crystals, which buckle into the third dimension around defect lines [16–18] in a manner directly analogous to the shapes we find. The buckled cores of defect lines are familiar to liquid crystal experimentalists. A second example is provided by deformable triangular latices, which have been studied extensively in the theory of two-dimensional melting. While the physical picture is different, the model energy is equivalent to a nematic membrane with isotropic elastic constants. Disclination defects culminating in a site with five or seven bonds (instead of the usual six) can lower their energy by buckling [19–22]. When draped over curved surfaces, collections of such defects arrange in specific patterns [23–26]. If surface tension is neglected, fivefold disclinations assume an approximately cone-shaped form [20].

In contrast to the above cases, competition between the cost of surface area and rod misalignment determines the shape of the defects we consider. When bending rigidity is neglected, we find that topological defects deform membranes into a simple universal shape known as a parabolic pseudosphere [27,28]. The size (height and extent) of this universal form is governed by the ratio of surface tension to in-plane elasticity. The inclusion of bending rigidity opposes this puckering. If the bending cost is small, the singularities at the tip and rim of the defect become smoother. The loga-

_____
[*]jrf@mit.edu

rithmically diverging tip of the parabolic pseudosphere is replaced by the finite height of an *elliptic* pseudosphere [28], and the sharp rim is replaced by an exponential falloff with a length scale related to the bending rigidity. Higher bending costs completely eliminate the buckling instability. The anisotropic elasticity of nematics singles out specific defect orientations (asters and vortices); and corresponding anisotropies in bending rigidity lead to different length scales for their shapes.

The rest of the paper is organized as follows. In Sec. II, we describe the free energy of a nematic membrane using tensor contractions from differential geometry. This provides a compact formulation applicable to all deformations, including highly curved shapes. In Sec. III, we describe vortex and aster defects, derive shape equations for radially symmetric configurations, and solve them to find the buckled defect shapes. Section IV provides a summary and indications for future research. In particular, we discuss aspects of experiments that could possibly be designed to observe these buckled shapes. In Appendix A, we study filament orientations in fixed geometries, which may provide other ways of measuring the nematic membrane parameters. In Appendix B, we check the linear stability of the buckled defect shapes.

II. ELASTIC FREE ENERGY OF NEMATIC MEMBRANES

Using differential geometry to describe a two-surface in three-space, we construct a power series expansion for the free energy by selecting a linearly independent set of scalar contractions of the surface tensors. For a surface described by an embedding vector $\vec{X}(\sigma^1, \sigma^2)$, one constructs tangent vectors $\vec{t}_i = \partial_i \vec{X}$ by taking derivatives of the embedding vector with respect to its two parameters. The metric tensor is then $g_{ij} = \vec{t}_i \cdot \vec{t}_j$. The covariant derivative is defined such that $D_i g_{jk} = 0$. The curvature tensor is constructed from covariant derivatives of the tangent vectors as $K_{ij} = (D_i \vec{t}_j) \cdot \hat{N}$, where $\hat{N}$ is a surface normal. One must choose a side to define the sign of $\hat{N}$. In the principal direction basis, $K_{ab} = \begin{pmatrix} 1/R_1 & 0 \\ 0 & 1/R_2 \end{pmatrix}$, where R_i are the radii of curvature [29].

A unit-magnitude tangent vector field $\vec{T} = T^i \vec{t}_i$ represents the nematic particles. At constant filament density, the magnitude $T^i T_i = 1$ is fixed and only its orientation changes.[1] Nematic symmetry implies invariance under $T^i \to -T^i$.[2] A complete set of scalars up to second order in derivatives is

$$\mathcal{F}_{\text{nematic}} = \sigma + \frac{K_1}{2}(D_i T^i)^2 + \frac{K_3}{2}(D_i T^j_\perp)^2 + \frac{\kappa_\parallel}{2}(T^i K_{ij} T^j - H_\parallel)^2$$

$$+ \frac{\kappa_\perp}{2}(T^i_\perp K_{ij} T^j_\perp - H_\perp)^2 + \frac{\kappa_\times}{2}(T^i K_{ij} T^j_\perp - H_\times)^2. \quad (1)$$

This free energy density must be integrated with a surface

area element $dA = \sqrt{g} d^2\sigma$, where g is the determinant of the metric. The weighted antisymmetric tensor $\gamma_{ij} = \sqrt{g} \epsilon_{ij}$ rotates one-tensors by $\pi/2$, such that $T^i_\perp = \gamma^{ij} T_j$ [29]. Note that $\gamma_{ij} g^{jk} \gamma_{kl} = -g_{il}$ and $D_i \gamma_{jk} = 0$. Each term is manifestly positive, so stability demands that the moduli be positive. In the remainder, we consider reflection-symmetric nonchiral membranes without spontaneous curvatures $H_{\parallel, \perp, \times}$.

Unlike parametrizations used to study nematic membranes near the hexatic fixed line [30,31], this set of scalars cleanly delineates the anisotropic bending energies that make nematic membranes unique. A linearized form of this free energy was written down by the Orsay Group [1] using rotations of the smectic director field to represent both smectic layer curvature and implicitly the director orientation. The relationship between the Orsay Group's linearized bulk model and a linearized two-dimensional model was clarified by Shalaginov [5]. Helfrich and Prost [2] used a nonlinearized form of these terms in studying membrane ribbons. Creating more surface area costs σ [32,33]. In-plane splay and bend cost K_1 and K_3, which are the two-dimensional analogs of the bulk nematic Frank constants [5,34]. Membrane curvature in the direction of the local filament orientation costs $\kappa_\parallel$ [30,31,35]. Curvature perpendicular to the filaments costs $\kappa_\perp$ [30,31]. These out-of-plane bending terms are the anisotropic analogs of the Canham [36] and Helfrich [37] bending rigidity. Saddle curves cannot be constructed from the other two out-of-plane bending terms and incur an independent energy cost of $\kappa_\times$. The square of the chiral scalar $TKT_\perp$ [2,30,38] is nonchiral. The underlying membrane has a fluid character in that the particles can rearrange in the surface without stretching or shearing costs.

Compared to the *splay*, *bend*, and *twist* of bulk nematics, nematic membranes have additional freedom that comes from relaxing a constraint: instead of three fields constrained to a unit vector, the nematic membrane constrains only two fields to a unit vector and allows a third field to range freely in describing the membrane's local deviation from flatness.[3]

In a system of motor proteins pulling on cytoskeletal filaments, K_1 would be proportional to motor density, which we assume to be uniform, and $\kappa_\perp$ would be determined primarily by the bare membrane's isotropic rigidity. Filament rigidity would influence both K_3 and $\kappa_\parallel$. See Appendix A for comments on $\kappa_\times$.

Perturbative renormalization group (RG) near the hexatic fixed line [31] shows that thermal fluctuations reduce weak anisotropy, i.e., the three quantities $\kappa_\times - \kappa_\parallel - \kappa_\perp$, $\kappa_\parallel - \kappa_\perp$, and $K_1 - K_3$ fade at long distances, so that only the hexatic membrane energy remains, and

$$\mathcal{F}_{\text{hexatic}} = \sigma + \frac{K_A}{2}(D_i T_j)(D^i T^j) + \frac{\kappa}{2}(K^i_i - H_0)^2, \quad (2)$$

where $K_A = \frac{1}{2}(K_1 + K_3)$ and $\kappa = \frac{1}{2}(\kappa_\parallel + \kappa_\perp)$. Under further rescaling, $\kappa \to 0$ and K_A is unrenormalized. Note that while the hexatic energy takes its name from the sixfold symmetry of

---

[1]Relaxing $T^i T_i = 1$ would introduce independent $TKKT$ and $T_\perp KKT_\perp$ terms and several new gradient terms.

[2]Dropping the nematic symmetry requirement introduces four new spontaneous curvatures, two of which are chiral.

[3]Such constraints deserve further study in the spirit of Capovilla and Guven's study of membranes with isotropic rigidity in Ref. [56].
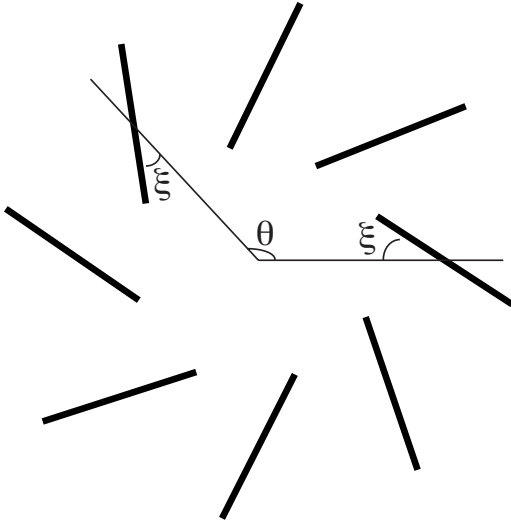
FIG. 1. Rod orientations around a general uniform +1 topological defect. $\xi=0$ corresponds to an aster, and $\xi=\pi/2$ to a vortex.

triangular lattices, any n-atic symmetry with $n\geq3$ restricts $K_1=K_3$ and $\kappa_\perp=\kappa_\parallel=2\kappa_\times$. For polar ($n=1$) or nematic ($n=2$) membranes, the isotropic approximation is an important limiting case at one extreme of a phase diagram that deserves further attention.

Since K_A is unrenormalized, patches of membrane material much larger than the thermal persistence length are well described by a free energy with only surface tension and the hexatic energy. Estimates of the thermal persistence length ξ_T of weakly anisotropic rigid membranes indicate an exponential form $\ln\xi_T\propto\kappa$ [31,39,40]. Modest changes in κ can thus sweep the persistence length from small values up to thousands of times the short-distance cutoff [41]. Shape distortions unique to the nematic membrane can then appear in patches of material smaller than this persistence length. In Sec. III, we derive the buckled shape of defects in both isotropic and anisotropic membranes. We also derive the shape modifications that result from bending rigidity $\{\kappa\}\neq0$ on these shapes. Given the wide range of experimentally observable thermal persistence lengths, one might find buckled defects of all these types.

III. BUCKLED DEFECT SHAPES

In the nematic phase, the rod orientation varies slowly throughout most of the material. However, at particular defect points, the orientation may be undefined, because rods at neighboring locations point in all directions. The *topological charge* of a defect is the number of times that the orientation rotates through 2π as the coordinate angle θ sweeps through 2π. Different patterns appear for integer, half-integer, and positive and negative charges. The defect depicted in Fig. 1 is radially symmetric, and is rotated by a uniform angle ξ with respect to the radial vectors.

In the limit of isotropic rigidity, +1 defects with any radially uniform ξ have the same energy. The symmetry is removed by the anisotropic moduli in a nematic membrane,

which distinguish asters ($\xi=0$) and vortices ($\xi=\pi/2$). The energy of such a planar defect as a function of ξ is

$$E_{\text{planar}}(\xi)=\pi[K_1\cos^2(\xi)+K_3\sin^2(\xi)]\ln\frac{R}{a}+E_c(\xi),\quad(3)$$

where R is the size of the membrane, a is a short-distance cutoff, and E_c is a core energy reflecting the defect's microscopic situation inside of the core radius a.

For $K_3>K_1$, asters have lower energy than vortices and are stable against in-plane deformations. If $K_1>2\kappa_\perp$, the defect energy is further reduced by buckling out of flatness to align the filaments in the third dimension. (See Appendix B for a linear stability analysis.) Buckling comes at the expense of creating more area, so surface tension sets the size of the deformation. Analogously, when $K_1>K_3>2\kappa_\parallel$, vortices are stable and can reduce their energy by tilting the surface around the defect.

To study this buckling, we minimize the nematic membrane energy, Eq. (1), around fixed aster and vortex arrangements. For a radially symmetric surface with no overhangs, we use the *polar Monge tangent* representation with embedding vector $\vec{X}(r,\theta)$. The height above the Monge plane is found by integrating the tangent angle $\chi(r)$ from a base value, so that

$$\vec{X}(r,\theta)=\begin{pmatrix}r\cos(\theta)\\r\sin(\theta)\\\int^r\tan[\chi(r')]dr'\end{pmatrix}.\qquad(4)$$

This yields a metric with no derivatives and thus lower-order shape equations. To handle shapes with overhangs, such as prolate vesicles [42], one can parametrize the shape by contour length instead of Monge radius.

The unit-vector constraint is enforced by defining the angle ξ such that

$$T^i=\begin{pmatrix}\cos(\xi)\cos(\chi)\\\sin(\xi)/r\end{pmatrix}.\qquad(5)$$

With this parametrization, the nematic membrane free energy becomes

$$\begin{aligned}F_{\text{nematic}}=2\pi\int dr\bigg(&\sigma\frac{r}{\cos(\chi)}+\frac{\cos(\chi)}{2r}\\&\times\{\kappa_\parallel[\sin^2(\xi)\tan^2(\chi)+r^2\cos^2(\xi)\chi'^2]\\&+\kappa_\perp[\cos^2(\xi)\tan^2(\chi)+r^2\sin^2(\xi)\chi'^2]\\&+\bar\kappa_\times\sin^2(\xi)\cos^2(\xi)[\tan(\chi)-r\chi']^2\\&+K_1[\cos(\xi)-r\sin(\xi)\xi']^2\\&+K_3[\sin(\xi)+r\cos(\xi)\xi']^2\}\bigg),\end{aligned}\qquad(6)$$

where $\bar\kappa_\times=\kappa_\times-\kappa_\parallel-\kappa_\perp$. We could have written the energy directly in terms of $\bar\kappa_\times$ by switching from a $(TKT)^2$ to a $TKKT$ parametrization as permitted by the unit-vector constraint. Fixed aster or vortex configurations carry no energy cost from the term proportional to $\bar\kappa_\times$. Setting to zero the

functional derivative of F_{nematic} with respect to χ yields a *shape equation*, which for an aster ($\xi=0$) becomes

$$0 = \sigma \frac{r \sin(\chi)}{\cos^2(\chi)} + \frac{\kappa_\parallel}{2} [-2 \cos(\chi)\chi' + r \sin(\chi)\chi'^2$$

$$-2r \cos(\chi)\chi''] + \frac{\kappa_\perp}{2}\left(1 + \frac{1}{\cos^2(\chi)}\right) \frac{\sin(\chi)}{r} - \frac{K_1}{2}\frac{\sin(\chi)}{r}. \tag{7}$$

For fixed vortices, the same shape equation holds after switching the coefficients $\kappa_\perp \leftrightarrow \kappa_\parallel$ and $K_1 \leftrightarrow K_3$.

For any membrane (hexatic or nematic) without stiffness ($\{\kappa\}=0$), defects have a simple universal shape resulting from the competition between the in-plane misalignment cost and surface tension. This can occur when the thermal persistence length is small compared to the system size, and thermal fluctuations have renormalized the stiffness to a small value. The misaligned rods near the defect core can align by bending out of the plane into the third dimension, at the cost of increasing surface area. The optimum tangent angle is given by the simple formula

$$\cos(\chi) = \sqrt{\frac{2\sigma r^2}{K_1}} = \frac{r}{r_0}, \tag{8}$$

where $r_0 = \sqrt{K_1/2\sigma}$ is the distance outside which surface tension dominates and flattens the surface. For a hexatic membrane, one would write K_A for K_1. Integrating the angle gives the universal shape

$$h(r) = r_0 \left[\text{sech}^{-1}\left(\frac{r}{r_0}\right) - \sqrt{1 - \left(\frac{r}{r_0}\right)^2} \right], \tag{9}$$

which approaches vertical at $r=0$ where the height is logarithmically divergent. This may be regulated by a cutoff, such as the membrane thickness. As a reference, at half the rim radius, $h(r_0/2) \approx 0.45 r_0$. In a hexatic membrane $K_1 = K_3 = K_A$, so asters and vortices have the same radius. In a nematic membrane, asters and vortices have different radii; the lower-energy defect also has smaller size.

The energy of this universal shape within the radius r_0 is equally divided between surface tension cost and splay cost,

$$E_{\text{buckled}} = 2\pi r_0^2 \sigma + \pi K_1 = 2\pi K_1. \tag{10}$$

Note that the surface area inside r_0 increases by exactly a factor of 2 over a flat disk. Interestingly, the logarithmic divergence of Eq. (3) disappears, and the energy is independent of the short-distance cutoff a. Thus, buckling lowers the energy of the defect.

This shape, Eq. (9), is known as a *parabolic pseudosphere* or *antisphere*, because it has constant negative Gaussian curvature equal to $-1/r_0^2$ [27,28]. It is also known as a *tractrisoid*, because it is half the surface of revolution generated by revolving a *tractrix* about its asymptote [43]. The tractrix is the path of an object being dragged by a string of constant length along a straight line that does not intersect the object. Leibniz likened this problem to a dog owner dragging his hound by its leash and named the solution *hundskurve*. The hundskurve has been studied by Huygens and others [44].
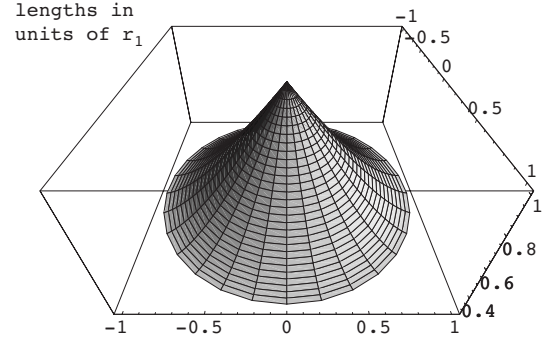

FIG. 2. An example elliptic pseudosphere for $r_1=1$ and $c=1$.

This construction makes it clear that the distance to the axis along the line tangent to any point on the surface is constant, i.e., the leash length is r_0. These shapes of constant negative curvature are also known in quantum gravity as solutions to classical Liouville theory [45].

This simple shape has singularities at the origin and at the rim $r=r_0$, which are modified by the membrane bending rigidities $\kappa_\perp$ and $\kappa_\parallel$, respectively. Setting $\kappa_\parallel=0$ removes all derivatives of χ from the shape equation, so a simple rearrangement provides the solution,

$$\cos(\chi) = \sqrt{\frac{2\sigma r^2 + \kappa_\perp}{K_1 - \kappa_\perp}} = \sqrt{\frac{(r/r_1)^2 + c}{1 + c}}, \tag{11}$$

where $r_1 = \sqrt{(K_1 - 2\kappa_\perp)/2\sigma}$ is the new rim radius, and $c = \kappa_\perp/(K_1 - 2\kappa_\perp)$ is related to the now finite slope at the tip. For sufficiently large K_1, the surface puckers out of the plane for $r < r_1$, with a profile

$$h(r) = \int_r^{r_1} \tan\left[\pm \cos^{-1}\left(\sqrt{\frac{2\sigma r^2 + \kappa_\perp}{K_1 - \kappa_\perp}}\right) \right] dr \tag{12}$$

$$= \pm r_1 \int_{r/r_1}^1 \sqrt{\frac{1 - u^2}{c + u^2}} du. \tag{13}$$

For $K_1 < 2\kappa_\perp$ or for $r_1 < r$, this solution is not real, so $\chi=0$ becomes the only solution to the shape equation.

Equation (13) is a complete elliptic integral of the second kind [46]. We change variables $u \to \sqrt{c} \sinh(u)$ to obtain

$$h(r) = \pm r_1 \sqrt{1 + c} \int \sqrt{1 - \frac{c \cosh^2(u)}{1 + c}} du, \tag{14}$$

where the integration ranges from $\sinh^{-1}[r/(r_1\sqrt{c})]$ to $\sinh^{-1}(1/\sqrt{c})$. In the study of surfaces with constant Gaussian curvature, Eq. (14) is a familiar expression for an elliptic pseudosphere [28]. Figure 2 shows an example elliptic pseudosphere.

Buckling into an elliptic pseudosphere also reduces the energy; however, the logarithmic divergence of the flat defect's energy, Eq. (3), reappears. While the particular formula for the energy of an elliptic pseudosphere is easy to calculate, it is long and we omit it.

The parabolic pseudosphere avoids a divergent energy near the core, Eq. (10), but has a logarithmically diverging tip height. The bending rigidity cuts off this tip height near

the core. Near the origin, the elliptic pseudosphere is approximately cone shaped with slope $\sqrt{1/c} = \sqrt{(K_1 - 2\kappa_\perp)/\kappa_\perp}$,

$$h(r) \rightarrow \pm \frac{r}{\sqrt{c}}. \tag{15}$$

If the r^2 term in Eq. (11) were not present, the shape would be a cone. Unlike the cone, pseudospheres have constant Gaussian curvature,

$$\frac{1}{R_1 R_2} = \det(K_i^j) = \det(\hat{N} \cdot \partial_i \vec{t}^j) \tag{16}$$

$$= -\frac{1}{r_1^2(1+c)}, \tag{17}$$

where $\hat{N}$ is the unit vector proportional to $\vec{t}_1 \times \vec{t}_2$ and we have carried through the computation after inserting the coordinate tangent vectors for the elliptic pseudoshere,

$$\vec{t}_1 = \left(\cos(\theta), \sin(\theta), \sqrt{\frac{1 - (r/r_1)^2}{c + (r/r_1)^2}} \right), \tag{18}$$

$$\vec{t}_2 = (-r\sin(\theta), r\cos(\theta), 0). \tag{19}$$

Even with finite $\kappa_\perp$ the above shape retains a cusplike singularity at the origin. We may well question how the singularity is modified by inclusion of cutoffs and higher-order terms. A simple short-distance cutoff a can be introduced as the radius of a hemispherical or similar cap over the singular point at the origin. The curvature energy density $\sim 1/a^2$ integrated over the cap's area $\sim a^2$ leads to a finite energy. We can then regard this as a benign singularity that adds a constant to the defect core energy E_c in Eq. (3).

Substituting Eq. (11) into the full shape equation, Eq. (7), leaves a term proportional to both $\kappa_\parallel$ and to r, so the elliptic pseudosphere is expected to remain valid as $r \rightarrow 0$ near the core. The situation at the rim is very different: Designating the distance from r_1 by $\epsilon = 1 - r/r_1$, one sees that $\chi \propto \sqrt{\epsilon}$ as $\epsilon \rightarrow 0^+$ and is zero immediately outside this radius. The abrupt rim would cause the energy proportional to $\kappa_\parallel$ to diverge, so when $\kappa_\parallel > 0$, the defect shape must be different. Since χ tends to zero away from the core, we linearize the shape equation for small χ and χ' to

$$0 \approx \left((K_1 - 2\kappa_\perp)\frac{1}{r} - 2\sigma r \right)\chi + 2\kappa_\parallel(\chi' + r\chi''). \tag{20}$$

After changing variables to ϵ and redefining $\chi \rightarrow \chi(\epsilon)$ to be a function of ϵ, the linearized shape equation is

$$0 = \epsilon(\epsilon - 2)\chi - \frac{2\kappa_\parallel(\epsilon - 1)}{K_1 - 2\kappa_\perp}[\chi' + (\epsilon - 1)\chi'']. \tag{21}$$

Note that the approximation is made for small χ and χ', and ϵ need not be small. For real-valued $\chi(\epsilon)$, this equation is solved by modified Bessel functions of the second kind with imaginary order. The order and argument both diverge with vanishing $\kappa_\parallel$, as
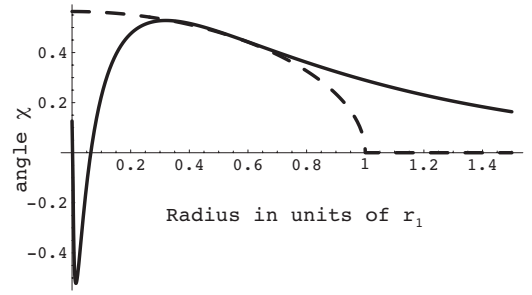

FIG. 3. Tangent angle (not the height) as a function of radius in units of r_1. Solid curve: The Bessel function solution for $\chi(\epsilon)$ for $\nu = 1$. Dashed curve: $\cos^{-1}\{\sqrt{[(r/r_1)^2 + c]/(1+c)}\}$ for $c = 2.5$ chosen to suggest matching in the crossover.

$$\chi(\epsilon) \propto K\left[i\nu, \nu\frac{r}{r_1} \right], \tag{22}$$

with

$$\nu = \sqrt{\frac{K_1 - 2\kappa_\perp}{2\kappa_\parallel}}. \tag{23}$$

This solution decays exponentially and has no zeros for $r_1 \leq r$. Since our parametrization does not handle overhanging surfaces, χ is limited to the range $(-\pi/2, \pi/2)$. Thus, for a given value of ν, the amplitude must be such that the solution stays in this range. For ν of order 1 and larger, an amplitude of unity yields a χ that is sufficiently small for $r_1 \leq r$ that the linearized shape equation is valid. It approaches zero asymptotically, so the rim radius at which $\chi = 0$ shifts to infinity. The asymptotic form of Eq. (22) is [47,48]

$$\chi \sim \frac{e^{-\sqrt{3/2}\nu r/r_1}}{\sqrt{\frac{r}{r_1}\nu}} \quad \text{for } (\nu, r) \rightarrow \infty, \tag{24}$$

which shows that bending rigidity introduces a new length scale

$$r_2 \equiv \sqrt{\frac{2}{3}}\frac{r_1}{\nu} = \sqrt{\frac{2\kappa_\parallel}{3\sigma}}. \tag{25}$$

As shown in Fig. 3, this solution for χ oscillates sharply near the core, which invalidates the small-χ' approximation. In this region, nonlinearities take over and the shape crosses over to the elliptic pseudosphere. As $\kappa_\parallel$ approaches zero, the Bessel function becomes flat for $r_1 < r$ and oscillates rapidly inside this radius, thus restoring the abrupt rim.

IV. CONCLUSIONS AND OUTLOOK

We predict that topological defects can buckle nematic membranes into elliptic pseudospheres with exponentially decaying rims. Let us explore this possibility in the case of a freely suspended thin film of smectic-C liquid crystal. The observation that these films maintain orientational order at room temperature suggests that K_1 (and K_3) are at least of the order of $k_B T_{\text{room}} \approx 4 \times 10^{-14}$ erg. If we assume a surface tension typical of *bulk* liquid crystal interfaces, σ

~ 10 erg/cm^2, and ignore bending rigidities ($\{\kappa\}=0$), then from $K \sim k_B T_{\text{room}}$, we would estimate a rim radius $r_0 = \sqrt{K/2\sigma} \approx 1/2$ nm, which is smaller than a typical film thickness and beyond the limits of this coarse-grained model. To create larger (observable) defects requires either smaller surface tension or larger in-plane stiffness than this initial estimate. Some physical systems may allow this.

For example, studies of thin films of liquid crystals often observe a small surface tension, because the chemical potential for particles in the film is similar to the chemical potential in the meniscus surrounding the film [32]. This reservoir on the edge of the suspended film allows the film to increase its area at a low energetic cost. One might control the size of buckled defects by manipulating the surface tension via this reservoir.

In addition to having a surface tension smaller than our initial estimate, some materials have observed values of $\{K\}$ one or two orders of magnitude larger than room temperature. For example, scattering studies by Spector *et al.* on thin films of smectic-C 4-(2–methylbutyl)-phenyl-4’-(octyloxy)-(1,1’)-biphenyl-4–carboxylate (8OSI) found large values of $\{K\}$ and surface tension made small by the meniscus [4]. This particular study used a smectic-C tilt angle of 32.2° and found $K_1/K_3 = 4.6(\pm 0.4)$, $\kappa_\parallel/K_3 = 3.4(\pm 0.3)$, $\kappa_\times/\kappa_\parallel = 5.5(\pm 3.1)$, $\kappa_\perp/\kappa_\parallel = 75(\pm 24)$, and $\kappa_\parallel \approx 10^{-12}$ erg. Unfortunately, the large value of $\kappa_\parallel/K_3$ prevents buckling. Since $K_1/K_3 > 1$, flat vortices should be stable relative to asters. For other tilt angles or other materials, one might hope to find lower values of $\kappa_\parallel/K_3$ that allow buckling.

For sufficiently floppy films, buckled defects could be observable via specular reflection or by interferometry techniques used to measure the flatness of mirrors. Additionally, islands of smectic-C material may provide means of manipulating single defects with laser tweezers, although coupling between the island’s multiple smectic layers may introduce additional effects [49].

While smectic-C 8OSI has sufficiently small surface tension and large in-plane stiffness, its bending rigidity suppresses buckling. That such shapes have not been observed so far in other materials may well be an indication of the importance of bending rigidity. Since typical lipid membranes have $\kappa \sim 5 k_B T_{\text{room}}$, this is a severe constraint. We note, however, that for stiff rods (nanotubes, cytoskeletal filaments) embedded in membranes, the rigidities $\kappa_\parallel$ and $\kappa_\perp$ and corresponding stiffnesses K_1 and K_3 may well differ by orders of magnitude. The challenge remains to obtain estimates of these parameters for specific microscopic models, and come up with an appropriate system for the study of buckled defects. Observations of these shapes in nematic membranes may provide estimates of the ratios between $\kappa_\perp$, $\kappa_\parallel$, K_1, K_3, and σ. Measurements of $\kappa_\times$ are possible via other shapes as described in Appendix A.

If one could control the anisotropic bending rigidities individually, one might be able to sweep a nematic membrane through a sequence of regimes in which different types of defects are stable. For example, for $K_3 < K_1$, if one could hold $\kappa_\parallel$ fixed while adjusting $\kappa_\perp$, one might observe buckled vortices when $2\kappa_\perp < K_1 - K_3 + 2\kappa_\parallel$, and buckled asters when $K_1 - K_3 + 2\kappa_\parallel < 2\kappa_\perp < K_1$, and buckled vortices again when $K_1 < 2\kappa_\perp$. By increasing $\kappa_\parallel$ while keeping $\kappa_\perp$ in any of these

regimes, one would flatten the preferred shape of vortices. Thus, it is possible for vortices and asters to prefer buckled or flat shapes independently.

In focusing on shapes of minimal energy, we have neglected thermal fluctuations. At long distances, thermal fluctuations reduce the differences between aster and vortex defects in *weakly* anisotropic membranes [31]. In future work, we would like to explore if this is still the case in *strongly* anisotropic membranes, or if thermal fluctuations can enhance the anisotropy.

Unlike bulk nematics, nematic sheets often appear with naturally periodic boundaries such as closed vesicles. By the Poincaré-Brouwer theorem [50], a genus-zero nematic vesicle must have topological charge of +2. In fact, defects can burst the vesicle [51–53]. This resembles *Bryopsis* sprouting branches out of defects in its tethered nematic cell wall—a topic to which we hope to return in the future.

APPENDIX A: NEMATIC MEMBRANES IN FIXED GEOMETRIES

While $\kappa_\times$ did not contribute to the shape of +1 defects, it affects other geometries. Following de Gennes’ molecular field argument [54], we impose the unit-vector constraint via a Lagrange multiplier λ and seek energy-minimizing filament configurations in fixed geometries. In a two-bein basis aligned with the principal directions, the curvature tensor is diagonal and $T^i = e_a^i T_a$, where e_a^i is a transformation to local coordinates in which $g_{ij} = \delta_{ij}$ at each point [29]. In the principal two-bein,

$$T_a = \begin{pmatrix} \cos(\xi) \\ \sin(\xi) \end{pmatrix}. \tag{A1}$$

In the following, there is no summation over a or $\bar{a} = (a+1)$ mod (2). The functional derivative of Eq. (1) in the principal two-bein reads

$$H_a \equiv \frac{\delta F}{\delta T_a} = -\lambda(\sigma^1, \sigma^2) T_a \tag{A2}$$

$$= T_a[\kappa_\parallel C_a^2 + \kappa_\perp C_{\bar{a}}^2 + \bar{\kappa}_\times T_{\bar{a}}^2 (C_1 - C_2)^2] - K_1 \partial_a (D_c T_c)$$
$$- K_3 \epsilon_{ba} \partial_b (\epsilon_{cd} D_c T_d) \tag{A3}$$

$$= T_a[\kappa_\parallel C_a^2 + \kappa_\perp C_{\bar{a}}^2 + \bar{\kappa}_\times T_{\bar{a}}^2 (C_1 - C_2)^2] - K_1 \partial_a (\partial_c \xi - A_c) T_{\perp c}$$
$$- K_3 \epsilon_{ba} \partial_b (\partial_c \xi - A_c) T_c, \tag{A4}$$

where C_a are the principal curvatures and $A_a = \hat{e}_1 \cdot \partial_a \hat{e}_2$ is the spin connection. The three-vectors $\hat{e}_a = e_a^i \vec{t}_i$ form an orthonormal basis in the principal two-bein. To set up the molecular

TABLE I. Stability criteria for various angles.

Angle	Stability criterion
$\xi=0$	$C_1\kappa_\parallel > C_2\kappa_\perp$
$\xi=\pi/2$	$C_1\kappa_\perp > C_2\kappa_\parallel$
$\cos^2(\xi) = \dfrac{C_1\kappa_\perp - C_2\kappa_\parallel}{(C_1 - C_2)(\kappa_\perp + \kappa_\parallel)}$	$C_1\kappa_\perp < C_2\kappa_\parallel,\ C_1\kappa_\parallel < C_2\kappa_\perp$

field equation, one must carry out the derivatives and pull out an overall factor of T_a to obtain an expression for λ that is a function of the index a. One obtains an equation for ξ by requiring λ to be a scalar, i.e., to have the same value for both $a=1$ and $a=2$. Solutions to this equation for ξ extremize the energy.

Considering first $K_1=0=K_3$, the equation yields a simple solution for ξ,

$$\cos^2(\xi) = \frac{1}{2}\left(1 + \frac{\kappa_\parallel - \kappa_\perp}{\kappa_\times - \kappa_\parallel - \kappa_\perp}\frac{C_1 + C_2}{C_1 - C_2}\right). \quad (A5)$$

This is valid only with both components of T_a nonzero, so $\xi=0$ and $\pi/2$ must also be considered in the list of possible ξ values. One must check which candidate value for ξ minimizes the energy for particular values of $\{\kappa\}$ and the principal curvatures. In the following, we list a few special cases. When $\kappa \equiv \kappa_\parallel = \kappa_\perp \neq \kappa_\times/2$ and $C_1 \neq C_2$, one has that $\xi=\pi/4$ minimizes the energy if

$$\frac{\kappa}{\kappa_\times} > -\frac{(C_1 - C_2)^2}{4C_1 C_2}. \quad (A6)$$

Otherwise, the filaments align with the least curved direction.

When $\kappa_\times = \kappa_\parallel + \kappa_\perp$, so that $\bar{\kappa}_\times = 0$, the orientation can be found by minimizing the energy with respect to ξ directly, instead of the molecular field equation. The result for $K_1 = 0 = K_3$ and $C_1 < C_2$ is shown in Table I.

On a developable surface, i.e., $C_1 = 0$ and $C_2 \neq 0$, when $\kappa_\times \geq 2\min\{\kappa_\parallel, \kappa_\perp\}$ the stable orientation is aligned with the uncurved direction. For smaller values of $\kappa_\times$, a special intermediate angle is the global minimum,

$$\cos^2(\xi) = \frac{2\kappa_\parallel - \kappa_\times}{2(\kappa_\parallel + \kappa_\perp - \kappa_\times)}. \quad (A7)$$

Note that this occurs only when both parallel and perpendicular bending are more costly than $\kappa_\times/2$. This might result from rods that weaken the sheet or have a specific texture on the rod's surface.

For a developable surface, the spin connection is zero, so the covariant derivatives become regular partial derivatives.

Thus, on a cylinder, far from boundaries, a constant orientation solves the full molecular field equation with the gradient terms included. This could allow experimental measurement of $(2\kappa_\parallel - \kappa_\times)/(\kappa_\parallel + \kappa_\perp - \kappa_\times)$.

In more general geometries, in-plane splay and bend compete with out-of-plane bending in a nonlinear partial differential equation, which, in principle, can be numerically integrated to fit model parameters to vectorized images of a real nematic membrane. The computation of model parameters from such images in the presence of topological defects requires care.

APPENDIX B: STABILITY OF BUCKLED DEFECT SHAPES

As discussed in Appendix A, the relative strength of $\kappa_\times$ plays an important role in the stability of orientation patterns on curved shapes. Substituting the principal curvatures for the elliptic pseudosphere into Eq. (A5) yields an equation for ξ that is not constant,

$$\cos^2(\xi) = \frac{2\kappa_\perp(r/r_1)^2 - \kappa_\times}{2(\kappa_\perp - \kappa_\times)}, \quad (B1)$$

and thus not the perfect aster (or vortex) that we assumed when setting up the shape equation, Eq. (7). Since Eq. (A5) was derived assuming $K_1=0=K_3$, the question remains whether the buckled defect is stable to perturbations away from a perfect aster (or vortex).

To check this, we construct linearized evolution equations for small perturbations,

$$\frac{d}{dt}\begin{pmatrix}\Delta \\ \Xi\end{pmatrix} \propto -\frac{\delta F}{\delta(\Delta,\Xi)} \approx M\begin{pmatrix}\Delta \\ \Xi\end{pmatrix}, \quad (B2)$$

where Δ represents deviations of the surface away from a pseudosphere, and Ξ represents deviations away from an aster ($\xi=0$). Perturbations of the height field couple with perturbations of the angle field, so all four components of the 2×2 matrix of differential operators, M, are nonzero. The perturbations are functions of both radius and angle, and are generally not radially symmetric. To solve this, we write the perturbations in a Fourier basis,

$$\begin{pmatrix}\Delta(r,\theta,t) \\ \Xi(r,\theta,t)\end{pmatrix} = \sum_m \begin{pmatrix}\Delta_m(r) \\ \Xi_m(r)\end{pmatrix}e^{im\theta}e^{\lambda_m t}, \quad (B3)$$

where each two-vector (Δ_m, Ξ_m) is independent. Substituting this solution into the evolution equation gives a separate set of coupled equations for each m value.

Neglecting bending rigidity, and choosing units of energy such that $\sigma=1$ and units of length such that $K_1=2\sigma$, we have for each value of m

$$M^{(m)} = \begin{bmatrix} \dfrac{r(-K_3 m^2 r + 2(1-r^2)[(2-4r^2)\partial_r + r(1-r^2)\partial_r^2])}{1-r^2} & \dfrac{im\{(2-K_3)r - [2-(2-K_3)r^2]\partial_r\}}{\sqrt{1-r^2}} \\ \dfrac{im\{K_3 r + (1-r^2)[2-(2-K_3)r^2]\partial_r\}}{r(1-r^2)^{3/2}} & -\dfrac{2m^2}{r^4} + K_3\partial_r^2 \end{bmatrix}. \quad (B4)$$

For $m=0$, the equations decouple. Since these are perturbations, we must find real-valued solutions that vanish at the boundaries $r=0$ and 1. The equation for Ξ has such a solution,

$$\Xi \propto \sin\left(r\sqrt{\frac{-\lambda_0}{K_3}}\right), \tag{B5}$$

if $\lambda_0 = -K_3\pi^2 n^2$ for integer n. This is always negative. The equation for Δ has the real-valued solution

$$\Delta \propto r^{2a} \,_2F_1\left(a, a+\frac{3}{2}; 2a+\frac{3}{2}; r^2\right)$$
$$+ r^{2b} \,_2F_1\left(b, b+\frac{3}{2}; 2b+\frac{3}{2}; r^2\right), \tag{B6}$$

where $_2F_1$ is the Gauss hypergeometric function and $a=(-1-\sqrt{1+2\lambda_0})/4$ and $b=(-1+\sqrt{1+2\lambda_0})/4$. Since the third argument exactly equals the sum of the first two, $0<r<1$ is the convergent domain for these functions. An *ad hoc* numerical study indicates that $\lambda_0 \to -\infty$ might extend this domain and allow the limit $\Delta(1) \to 0$. These functions also diverge at $r=0$, and again a large negative λ_0 appears to mediate this because the function oscillates rapidly and might average to zero as $r \to 0$. We lack an analytic treatment

of this asymptotic regime, so we turn to a numerical method below.

Considering $0<m$ and substituting $u=r^2$, one sees that Eq. (B4) consists of second-order ordinary differential equations with nonessential singularities at two points (the boundaries), so the equations can be transformed into hypergeometric differential equations [55]. By combining linearly independent solutions, one might construct real solutions that meet the boundary conditions for all values of m. After satisfying these constraints, one would obtain expressions for λ_m, which, when negative, indicate stable regions of parameter space. This approach is complicated even when rigidity is neglected.

Instead of taking this approach, we have checked stability numerically by discretizing the fields. We represent the deviations of the height and angle fields by a large column vector of field values at discrete steps in radius and polar angle. By representing the derivative operators as banded square matrices acting on this large vector, one obtains a matrix of numbers for any given set of parameter values. The largest nonzero eigenvalue of this matrix determines the stability of the shape. If the largest nonzero eigenvalue is negative, then that set of parameters suppresses perturbations and the shape remains stable.

We have carried out such a numerical procedure. Generally, the buckled aster is stable for $2\kappa_\perp < K_1 < K_3$ and any $0 < \kappa_\times$. The analogous statement holds for buckled vortices.

---

[1] Orsay Group on Liquid Crystals, Solid State Commun. **9**, 653 (1971).

[2] W. Helfrich and J. Prost, Phys. Rev. A **38**, 3065 (1988).

[3] C. Y. Young, R. Pindak, N. A. Clark, and R. B. Meyer, Phys. Rev. Lett. **40**, 773 (1978).

[4] M. S. Spector, S. Sprunt, and J. D. Litster, Phys. Rev. E **47**, 1101 (1993).

[5] A. N. Shalaginov, Phys. Rev. E **53**, 3623 (1996).

[6] M. F. Islam, A. M. Alsayed, Z. Dogic, J. Zhang, T. C. Lubensky, and A. G. Yodh, Phys. Rev. Lett. **92**, 088303 (2004).

[7] G. Yu, A. Cao, and C. M. Lieber, Nat. Nanotechnol. **2**, 372 (2007).

[8] J. B. Fournier and L. Peliti, Phys. Rev. E **58**, R6919 (1998).

[9] Y. Fukui and S. Inoue, Cell Motil. Cytoskeleton **18**, 41 (1991).

[10] F. Nedelec, T. Surrey, A. Maggs, and S. Leibler, Nature (London) **389**, 305 (1997).

[11] T. Surrey, F. Nedelec, S. Leibler, and E. Karsenti, Science **292**, 1167 (2001).

[12] M. C. Lagomarsino, Ph.D. thesis, University of Leiden, 2004 (unpublished).

[13] H. Y. Lee and M. Kardar, Phys. Rev. E **64**, 056113 (2001).

[14] A. Zumdieck, M. C. Lagomarsino, C. Tanase, K. Kruse, B. Mulder, M. Dogterom, and F. Julicher, Phys. Rev. Lett. **95**, 258103 (2005).

[15] P. Green, Am. J. Bot. **47**, 476 (1960).

[16] P. Cladis and M. Kleman, J. Phys. (Paris) **33**, 591 (1972).

[17] R. B. Meyer, Philos. Mag. **27**, 405 (1973).

[18] S. Anisimov and I. Dzyaloshinskii, Sov. Phys. JETP **36**, 774 (1973).

[19] D. Nelson and L. Peliti, J. Phys. (Paris) **48**, 1085 (1987).

[20] H. S. Seung and D. R. Nelson, Phys. Rev. A **38**, 1005 (1988).

[21] D. R. Nelson, in *Fluctuating Geometries in Statistical Mechanics and Field Theory*, edited by F. David, P. Ginsparg, and J. Zinn-Jusin, Proceedings of the Les Houches Summer School of Theoretical Physics, LXII (Elsevier Science, Amsterdam, 1994), Chap. 5.

[22] D. R. Nelson, *Defects and Geometry in Condensed Matter Physics* (Cambridge University Press, Cambridge, U.K., 2002).

[23] V. Vitelli and A. M. Turner, Phys. Rev. Lett. **93**, 215301 (2004).

[24] V. Vitelli and D. R. Nelson, Phys. Rev. E **70**, 051105 (2004).

[25] V. Vitelli, J. B. Lucks, and D. R. Nelson, Proc. Natl. Acad. Sci. U.S.A. **103**, 12323 (2006).

[26] V. Vitelli and D. R. Nelson, Phys. Rev. E **74**, 021711 (2006).

[27] E. W. Weisstein, ttp://mathworld.wolfram.com/Pseudosphere.html

[28] E. Kreyszig, *Differential Geometry* (Dover Publications, New York, 1991).

[29] F. David, *Statistical Mechanics of Membranes*, 2nd ed. (World Scientific, Singapore, 2003), Chap. 7.

[30] P. Nelson and T. Powers, Phys. Rev. Lett. **69**, 3409 (1992).

[31] T. Powers and P. Nelson, J. Phys. II **5**, 1671 (1995).

[32] F. Brochard, P. de Gennes, and P. Pfeuty, J. Phys. (Paris) **37**, 1099 (1976).

[33] F. David and S. Leibler, J. Phys. II **1**, 959 (1991).

[34] F. C. Frank, Discuss. Faraday Soc. **25**, 19 (1958).

[35] X. Xing, e-print, arXiv:0708.3182.

[36] P. Canham, J. Theor. Biol. **26**, 61 (1970).

[37] W. Helfrich, Z. Naturforsch. C **28c**, 693 (1973).

[38] P. Nelson and T. Powers, J. Phys. II **3**, 1535 (1993).

[39] H. Kleinert, Phys. Lett. **114A**, 263 (1986).

[40] P. Gutjahr, R. Lipowsky, and J. Kierfeld, Europhys. Lett. **76**, 994 (2006).

[41] P. de Gennes and C. Taupin, J. Phys. Chem. **86**, 2294 (1982).

[42] U. Seifert, K. Berndl, and R. Lipowsky, Phys. Rev. A **44**, 1182 (1991).

[43] E. W. Weisstein, http://mathworld.wolfram.com/Tractrix.html

[44] E. Lockwood, *A Book of Curves* (Cambridge University Press, Cambridge, U.K., 1961).

[45] N. Seiberg, Prog. Theor. Phys. Suppl. **102**, 319 (1990).

[46] E. W. Weisstein, http://mathworld.wolfram.com/CompleteEllipticIntegraloftheSecondKind.html

[47] C. B. Balogh, SIAM J. Appl. Math. **15**, 1315 (1967).

[48] *Handbook of Mathematical Functions*, edited by M. Abramowitz and I. A. Stegun (Dover, New York, 1972).

[49] A. Pattanaporkratana, C. S. Park, J. E. Maclennan, and N. A. Clark, Ferroelectrics **310**, 131 (2004).

[50] R. D. Kamien, Rev. Mod. Phys. **74**, 953 (2002).

[51] F. C. MacKintosh and T. C. Lubensky, Phys. Rev. Lett. **67**, 1169 (1991).

[52] J. M. Park, Phys. Rev. E **54**, 5414 (1996).

[53] R. M. L. Evans, Phys. Rev. E **53**, 935 (1996).

[54] P. G. de Gennes, *The Physics of Liquid Crystals* (Oxford University Press, Oxford, 1993).

[55] E. W. Weisstein, http://mathworld.wolfram.com/HypergeometricDifferentialEquation.html

[56] R. Capovilla and J. Guven, J. Phys. A **38**, 2593 (2005).